Title

Interactions, Transformations, and Bioavailability of Nano-Copper Exposed to Root Exudates

Journal

Environmental Science and Technology, 51(17)

ISSN

0013-936X

Authors

Huang, Yuxiong
Zhao, Lijuan
Keller, Arturo A

Publication Date

2017-09-05

DOI

10.1021/acs.est.7b02523

Peer reviewed

Environmental Science & Technology

Article

pubs.acs.org/est

Interactions, Transformations, and Bioavailability of Nano-Copper Exposed to Root Exudates

Yuxiong Huang,[†,‡] Lijuan Zhao,[†,‡] and Arturo A. Keller*[,†,‡]

[†]Bren School of Environmental Science and Management, University of California at Santa Barbara, Santa Barbara, California 93106, United States

[‡]Center for Environmental Implications of Nanotechnology, University of California, Santa Barbara, California 93106, United States

Supporting Information

ABSTRACT: Due to the potential for interactions between crop plants and engineered nanomaterials (ENMs), there is increasing interest in understanding the bioavailability and effects of ENMs released into soil systems. Here, we investigate the influence of root exudates on the fate of ENMs from a thermodynamic perspective. Nano isothermal titration calorimetry was applied to determine thermodynamic parameters for the interaction between nanocopper (*n*Cu) and synthetic root exudate (SRE) and its components (including sugars, organic acids, amino acids, and phenolic acids), as well as Cu^{2+} and SRE. The measured binding constant (K_d = 5.645 × 10^3 M^{-1}) indicated strong interactions between *n*Cu particles and SRE, as well as with individual organic acids. The interaction between Cu^{2+} and SRE was stronger (K_d = 7.181 × 10^4 M^{-1}) but varies for the individual SRE components. *n*Cu dissolution in the presence of SRE was the predominant interaction. In addition, SRE resulted in a complex transformation of *n*Cu, where Cu^{2+}, Cu^{+}, and Cu^{0} were formed via oxidation and reduction. Plant−*n*Cu exposure experiments indicate that the binding of SRE with *n*Cu and dissolved Cu ions can significantly decrease Cu uptake and bioaccumulation in plants. nITC provides a fundamental thermodynamic understanding of interactions between *n*Cu and plant root exudates, providing an important tool for understanding plant NP-interactions.

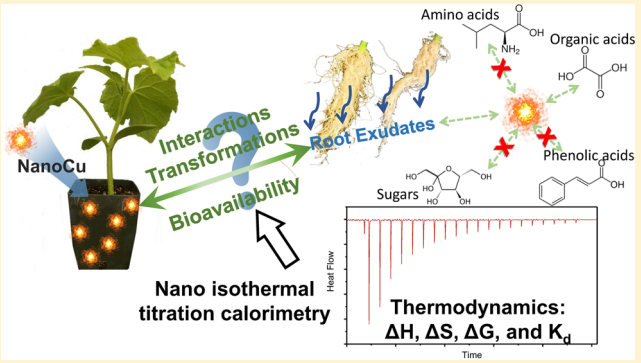

INTRODUCTION

Copper-based nanoparticles (Cu NPs) have many current and potential applications in engineering, agriculture, and other fields.[1−4] Global production of Cu NPs in 2010 was estimated at ∼200 t/yr.[5] A large fraction of these Cu NPs may end up in landfills, but a fraction may be released into soils and water bodies, particularly from copper-based pesticides and via biosolids.[2,5−7] Cu NPs in the soil may impact crop plants.[8−15]

However, there is a need to better understand the bioavailability of the NPs, as well as the interactions between plants, plant-derived biomolecules, and NPs.

Nearly 5% to 21% of all photosynthetically fixed carbon is transferred to the rhizosphere through root exudates (RE), which assist the plant in nutrient acquisition from the soil with the development of the microbiome in the rhizosphere.[16−18] RE are comprised of low molecular weight compounds such as amino acids, organic acids, sugars, phenolic, and various other secondary metabolites and high molecular weight compounds (e.g., polysaccharides and proteins).[19] The impact of the wide variety of RE compounds on the fate and behavior of NPs in terrestrial ecosystems is likely significant but poorly understood.[20,21] The stability and dissolution of NPs in the environment depend on solution chemistry, including ionic strength, pH, and natural organic matter concentration ([NOM]),[7,22,23] and physicochemical properties of NPs, such as size, coating, and solubility, have significant implication on their toxicity.[6,7,24] RE compounds can be a significant fraction of NOM in agricultural soils, particularly near the root zone, and may alter pH and even ionic strength (IS), as well as enhance microbial activity, which will likely affect the fate of NPs in this region.

As an example of the interactions between RE and NPs, amino acids from cucumber plant roots were shown to decrease plant uptake of Cu^{2+} and *n*Cu.[25] In contrast, organic acids from RE in rhizosphere may decrease soil pH and enhance the dissolution of *n*Cu, thus improving the bioavailability of Cu^{2+}. Complicating matters, some organic acids and amino acids may act as ligands to complex with Cu ions or Cu NPs and hinder their uptake by the plant.[25] RE can also participate in a number of redox reactions. Consequently, the presence of RE will most likely influence the fate and transport of NPs, including their retention, dissolution, and other transformations.[21]

Received: May 16, 2017
Revised: July 26, 2017
Accepted: August 3, 2017
Published: August 3, 2017

DOI: 10.1021/acs.est.7b02523
Environ. Sci. Technol. XXXX, XXX, XXX−XXX

nITC has a much higher resolution than traditional ITC and has recently been applied in the field of environmental science and engineering as it can directly measure the heat absorbed or released during interactions (e.g., bond formation).[26−28] nITC provides accurate, rapid, and label-free thermodynamic data on the changes in enthalpy (ΔH), entropy (ΔS), and Gibbs free energy (ΔG) of the interaction. The affinity binding constant K_d and the interaction reaction stoichiometry can be also determined in a single titration experiment.[29] Thus, nITC is a novel approach to investigate the thermodynamics of plant−ENM interactions, particularly in the presence of RE.

In this study, synthetic root exudates (SRE) were used to study their effect on the fate of *n*Cu particles in soil and plants. We applied nITC to obtain key quantitative thermodynamic data of the interactions between SRE (as a mixture and its individual components) and *n*Cu particles, as well as SRE and Cu^{2+} ions, to better understand the dominant mechanisms in the binding process. The chemical state of *n*Cu after the interaction with SRE (both mixture and individual components) was also studied to understand the transformation caused by SRE. Furthermore, using cucumber plants exposed to *n*Cu, we investigated the availability of free Cu ion in the soil and the bioaccumulation of Cu in the plants in the presence of SRE.

MATERIALS AND METHODS

Characteristics of *n*Cu. Uncoated *n*Cu (U.S. Research Nanomaterials) was employed here; a detailed characterization was presented in a previous study.[7] Briefly, the primary particle size is 40 nm, and the hydrodynamic diameter (HDD) is 2590 ± 1138 nm in deionized (DI, Barnstead nanopure) water at pH 7 (0.5 mM phosphate buffer), at similar concentrations as in this study. Scanning electron microscopy (SEM) and transmission electron microscopy (TEM) images of *n*Cu are presented in the SI (Figure S1). The surface charge, expressed as zeta potential in a 0.5 mM phosphate buffer solution, is −29.4 ± 0.8 mV at pH 7.

Synthetic Root Exudates (SRE). A synthetic root exudate (SRE) solution was prepared, using a filter-sterilized mix of low molecular weight organics previously reported to occur in plant root exudates,[20] as shown in Table S1. In the current study, the prepared SRE was used as a model to study the mechanism of the interactions between *n*Cu and SRE. However, the concentrations and components of RE are likely to change as a function of plant species, life cycle stage, and soil type. In addition, the microbiome in the rhizosphere may affect the composition of RE due to the microbial exudates and microbial degradation of plant exudates.[30]

Isothermal Titration Calorimetry Measurement. A TA Instruments Nano Isothermal Titration Calorimeter (nITC) instrument (TA Instruments-Waters LLC, DE, US) was used to measure the heat exchange between *n*Cu or Cu^{2+} and SRE (mixture and individual compounds) at 298 K to determine the thermodynamic data and binding constants.

***n*Cu nITC Measurements.** A *n*Cu suspension, prepared in degassed DI water (pH 7), was freshly made from powdered *n*Cu before the nITC measurements to minimize the contribution from dissolved Cu^{2+}. The *n*Cu (1.31 mM/L) suspension was placed in the 1 mL nITC sample cell. The rotational speed of the stirrer was 250 min^{-1} to ensure *n*Cu was well suspended, and a solution of either SRE mixture or individual components was loaded into the 100 μL injection syringe. (Concentrations are listed in Table S2, and the concentrations of SRE components were generally 10 times higher than the concentration of *n*Cu to obtain a strong heat exchange signal as well as to ensure reaching interaction equilibrium. The difference in concentrations ratio would not change the output significantly.[31]) SRE or its components were titrated into the sample cell as a sequence of 20 injections of 4.91 μL aliquots. The equilibrium time between two injections was set at 1600 s for the signal to return to the baseline. Estimated binding parameters were obtained from the nITC data using the NanoAnalyze Data Analysis software (Version 3.60) and modeling as described in the SI.

Cu^{2+} nITC Measurements. A solution of either the SRE mixture or its individual components (concentrations are listed in Table S3), prepared in degassed DI water, was placed in the 1 mL nITC sample cell, and a Cu^{2+} solution (20 mM/L) was loaded into the 100 μL injection syringe. Cu^{2+} was titrated into the sample cell as a sequence of 20 injections of 4.91 μL aliquots. The rotational speed of the stirrer was 250 min^{-1}, and the equilibrium time between two injections was set at 800 s for the signal to return to the baseline.

Transformation of *n*Cu. To study *n*Cu transformations, 40 mg of *n*Cu was suspended in 40 mL of different solutions, including DI water, the SRE mixture, and individual organic acids (12.5 mM citric, malic, oxalic, and succinic acids). After mixing for 48 h to allow for equilibration, the solid fractions (which included *n*Cu particles and Cu salt precipitates) were separated from the aqueous phase and analyzed via X-ray photoelectron spectroscopy (XPS, Kratos Axis Ultra) and Fourier transform infrared (FTIR) spectrometry (Nicolet iS10). To prepare the sample, the solid fractions were separated from the suspension via centrifugation (10 000g, 30 min). Particles were immediately dried under vacuum (Yamato ADP-21) after decanting the supernatant. The Cu concentration in the supernatant was analyzed by ICP-MS (Agilent 7900, Agilent Technologies, Santa Clara, CA), and solution pH was monitored before and after mixing. HDD and zeta potential of *n*Cu particles after exposed to SRE were measured by dynamic light scattering (Malvern Zetasizer Nano-ZS90).

Influence of SRE on Bioavailability of *n*Cu in Soil. Batch studies were conducted to investigate the bioavailability of free Cu ions in the soil after *n*Cu was exposed to SRE or individual organic acids. The soil was collected from the Natural Reserve System of UC Santa Barbara (Sedgwick), and the soil composition was reported in a previous study.[6] Generally, 4 mg of *n*Cu particles were mixed with 5 g of soil containing 1 mL of SRE solution or individual organic acids (citric, malic, oxalic, and succinic acids) spiked in 50 mL conical tubes, and then, the tubes were filled to 50 mL with DI water. Afterward, these tubes were mixed in an end-over-end shaker on a Dayton-6Z412A Parallel Shaft (USA) roller mixer with a speed of 70 rpm at room temperature for 7 days to ensure sufficient equilibration time. The availability of free Cu ions was determined by ICP-MS by analyzing [Cu] in the supernatant separated via centrifugation (10 000g, 30 min). Solution pH was monitored before and after mixing. All tests were performed in triplicate, and analysis of variance (ANOVA) was used to test the significance of results. A $p < 0.05$ was considered to be statistically significant.

Influence of SRE on Bioaccumulation of Cu in Plants. Cucumber (*Cucumis sativus*) seeds were purchased from Seed Savers Exchange (Iowa, USA). *n*Cu was suspended in DI water and sonicated for 30 min before being applied to the soil (Sedgwick soil). The final concentration of *n*Cu in soil was 0

DOI: 10.1021/acs.est.7b02523
Environ. Sci. Technol. XXXX, XXX, XXX−XXX

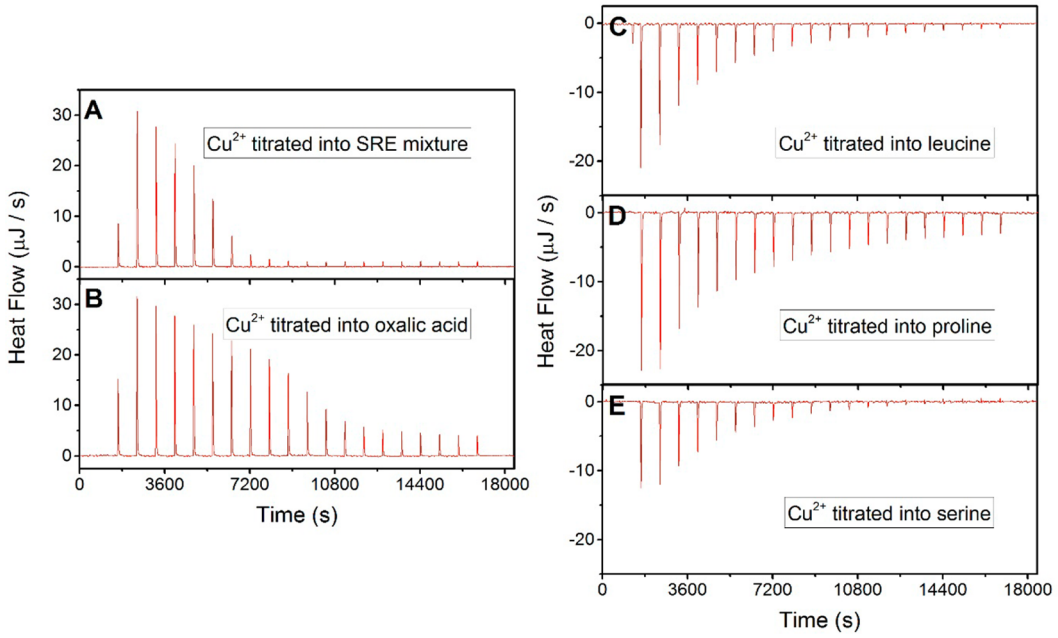

Figure 1. Thermograms for Cu^{2+} titration into (A) SRE, (B) oxalic acid, (C) proline, (D) leucine, and (E) serine solutions at 298 K. Heat flow reflects the differential signal, with negative peaks indicating an endothermic process and positive peaks indicating an exothermic process.

(control) and 800 mg/kg. This total Cu concentration is within the range predicted for biosolids applied to soils[32] or due to the application of copper-based nanopesticides.[33] Each treatment had four replicates. In each replicate, pairs of cucumber seedlings were grown in 3.0 L Poly-Tainer containers. For the SRE treatment, 0 (control) and 5 mL of SRE mixture was added to the soil in the first 30 days. The cucumber plants were grown 60 days in the greenhouse at a controlled temperature from 25.5 to 30.0 °C during the day and 17.7 to 18.9 °C at night. At harvest, the cucumber leaves were oven-dried for 7 days at 60 °C. The oven-dried tissues were ground to powder and digested with HNO_3 and H_2O_2 (1:4) using a microwave oven system (Multiwave Eco, Anton Parr). The digestion method was based on EPA 3051.[34] Standard reference materials, NIST 1547 (peach leaves) and 1570a (spinach leaves), were also used to analyze the samples. The recoveries for all elements were between 90% and 99%.[35] The mineral nutrient elements were analyzed using ICP-MS.

RESULTS AND DISCUSSION

Determination of Cu^{2+}–SRE Thermodynamic Binding Parameters by nITC. The heat exchange as a function of time as Cu^{2+} is titrated into the SRE solution is shown in the real-time thermogram (Figure 1). Each injection of Cu^{2+} results in heat change due to the binding between Cu^{2+} and SRE within the sample cell, causing a change in the heat flow, shown as peaks in the thermogram (Figure 1). The interaction between $Cu^{2+}$and SRE (Figure 1A) or oxalic acid (Figure 1B) is exothermic, while titration of Cu^{2+} into amino acids (Figure 1C, D, and E) indicates an endothermic reaction. Peak amplitudes and area gradually decrease as more Cu^{2+} is added since the number of available binding sites decreases. Eventually, only a low heat exchange is observed for the last several injections corresponding to dilution, once binding sites are saturated. Compared to the strong interaction between Cu^{2+} and oxalic acid or select amino acids, nITC measurements of the titration of Cu^{2+} into other SRE components (sugars, phenolic acidsand small organic acids) resulted in a low exothermic interaction, similar to the titration of Cu^{2+} into water, reflecting only dilution heat, as shown in Figure S2.

The energy exchange as a function of the ratio between Cu^{2+} and SRE, oxalic acid, and three amino acids is presented in Figure 2. The independent set of multiple binding sites (MNIS) model[36] (eq S1) was applied to process the data, and all the fitted and calculated thermodynamic parameters are listed in Table 1. All studied interactions are energetically favored with spontaneous processes at 298 K with negative changes in Gibbs free energy (ΔG), ranging from −18.91 to −27.72 kJ/mol (Table 1). The main driving process for the Cu^{2+}–SRE interaction is the significant gain in entropy ($-T\Delta S < \Delta H$), as shown in Table 1.

For the amino acids (AAs) studied, formation of the Cu^{2+}–AAs complexes is only entropically driven but not both enthalpically and entropically favored, suggested by the positive ΔS and positive ΔH values (Table 1). The changes in the entropy (ΔS) varied from 110.8 to 132.2 J/mol K, which are close to the ΔS values found for the reaction $2AA^- + Cu^{2+} \rightleftharpoons Cu(AA)_2$, which range from ∼110 to ∼130 J/mol K.[37] Furthermore, the stoichiometric values are close to 0.5 (n = 0.486, 0.472, and 0.324 for serine, proline, and leucine, respectively), which suggests that the major complex formed is $Cu(AA)_2$. Notably, the stoichiometric value (n) is smaller for leucine, which may reflect leucine's larger molecular size; conformational hindrance may restrict Cu^{2+} access. Thus, for Cu^{2+}–leucine complexation, the dominant process may involve both $Cu(AA)_2$ and $[Cu(AA)]^+$. The positive enthalpy ($\Delta H > 0$) values could be contributed by the dehydration of AA, resulting from the release of coordinated water molecules upon binding of the AAs to the Cu^{2+}, which is endothermic.[38] Therefore, the process could more accurately be described as $2AA - (H_2O)_x + Cu^{2+} \rightleftharpoons Cu(AA)_2 - (H_2O)_y + zH_2O$. Of these three AAs, leucine is the most hydrophobic, based on its n-octanol—water (K_{ow}) partition coefficient ($\log K_{ow} = -1.61 \pm 0.08$), while serine is the most hydrophilic ($\log K_{ow} = -3.30$

DOI: 10.1021/acs.est.7b02523
Environ. Sci. Technol. XXXX, XXX, XXX−XXX

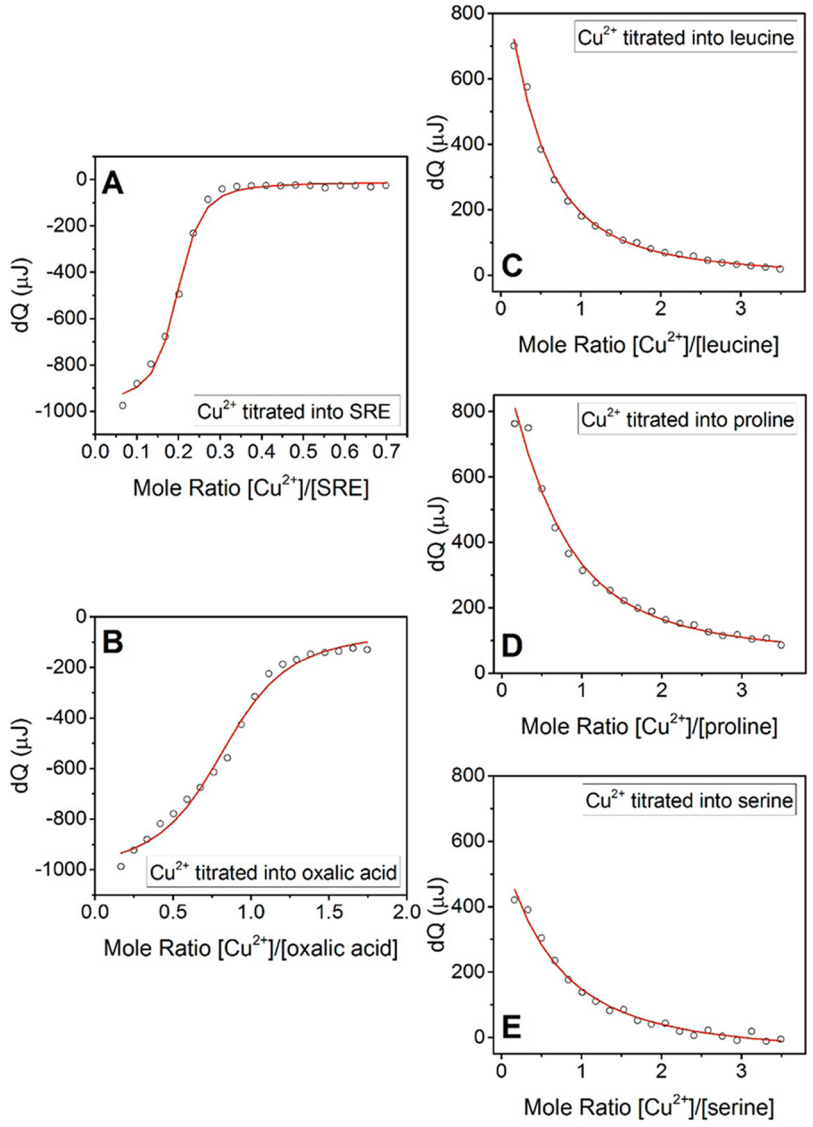

Figure 2. Integrated heat data as a function of mole ratio of Cu^{2+} to (A) SRE, (B) oxalic acid, (C) leucine, (D) proline, and (E) serine, fitted with MNIS model. Symbols represent experimental data, and red lines represent model prediction.

Table 1. MNIS Model Fit of ΔH and n with Confidence Intervals (95% confidence level) from nITC Analysis of the Interaction between SRE or Its Components and Cu^{2+} and Calculated K_d, ΔG, ΔS, and $-T\Delta S$ from K_a and ΔH Values

Components	ΔH (kJ/mol)	n	K_d (M^{-1})	ΔG (kJ/mol)	ΔS (J/K mol)	$-T\Delta S$(kJ/mol)
SRE	−9.696 ± 0.567	0.186 ± 0.006	7.181×10^4	−27.72	60.45	−18.02
Oxalic acid	−9.863 ± 0.923	0.839 ± 0.049	1.372×10^4	−23.62	46.13	−13.75
Proline	20.09 ± 4.73	0.472 ± 0.031	2.429×10^3	−19.32	132.2	−39.41
Leucine	19.00 ± 3.45	0.324 ± 0.018	3.731×10^3	−20.39	132.1	−39.39
Serine	14.13 ± 0.76	0.486 ± 0.012	2.054×10^3	−18.91	110.8	−33.04

± 0.12).[39] Thus, serine has a significantly smaller ΔS value (Table 1), indicating that less water molecules are released upon binding than for the other more hydrophobic AAs. Serine also has a smaller enthalpy change (ΔH) value, also reflecting its lower hydrophobicity.

The binding enthalpy is favorable ($\Delta H < 0$) for the formation of Cu complexes with both oxalic acid and SRE. The significantly smaller entropy changes indicate that there is a much smaller dehydration associated with oxalic acid and SRE. For oxalic acid, $n = 0.839$, which is slightly lower than unity; thus, the complex reaction involves a combination of the following equilibria:[40] $Cu^{2+} + HC_2O_4^- \rightleftharpoons CuC_2O_4^+$, $Cu^{2+} + C_2O_4^{2-} \rightleftharpoons CuC_2O_4$, and $CuC_2O_4 + C_2O_4^{2-} \rightleftharpoons Cu(C_2O_4)_2^{2-}$. For the SRE mixture, n is considerably lower than unity ($n = 0.186$), indicating multiple SRE components may be binding with Cu^{2+}, forming mixed ligand chelates of Cu^{2+}−SRE, with the following possible interactions: $Cu^{2+} + A^{2-} \rightleftharpoons CuA$, $CuA + L \rightleftharpoons CuA$ and $Cu^{2+} + A^{2-} + L \rightleftharpoons CuA$, where A and L represent the acids and ligands in SRE, for example, oxalic acid[41] and amino groups,[42,43] respectively.

The affinity to Cu^{2+} follows the pattern SRE > oxalic acid > leucine > proline > serine (Table 1). SRE has the strongest

DOI: 10.1021/acs.est.7b02523
Environ. Sci. Technol. XXXX, XXX, XXX−XXX

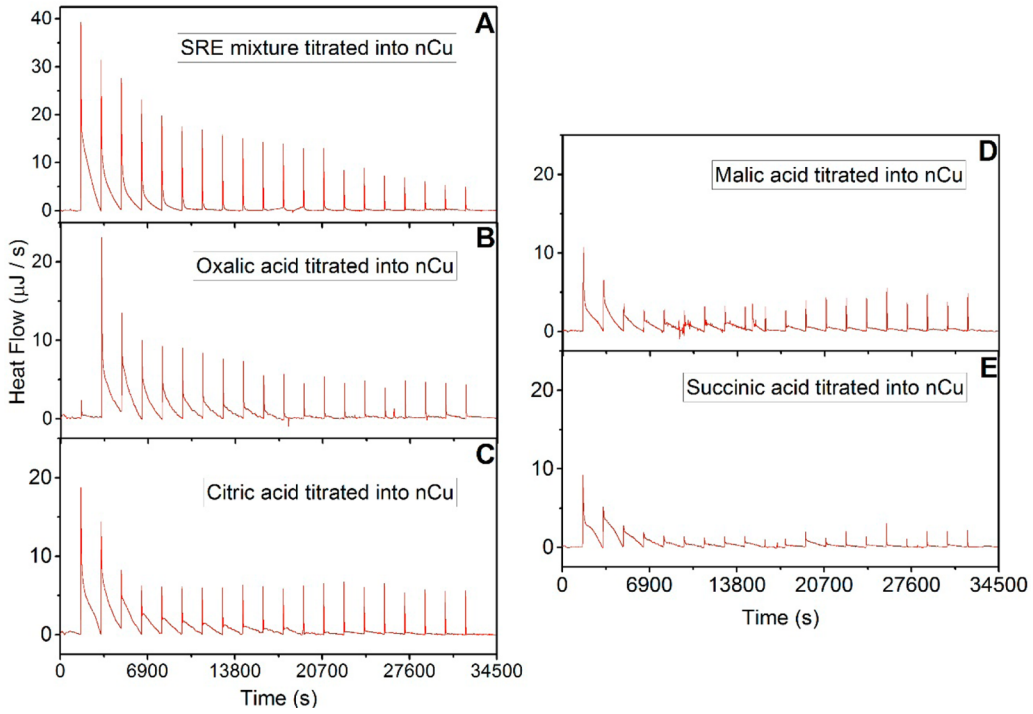

Figure 3. Real-time thermogram for titration of (A) SRE, (B) oxalic acid, (C) citric acid, (D) malic acid, and (E) succinic acid into the *n*Cu suspension at 298 K.

interaction with Cu^{2+}, with a binding constant of 7.181×10^4 M^{-1}, while all the amino acids showed much weaker affinity, with serine having the weakest binding constant of 2.054×10^3 M^{-1}, more than a 10-fold difference. Previous studies suggest amino acids bind Cu^{2+} to the nitrogen atom of the amino group and to an oxygen atom in carboxylate, which would result in lower binding constants.[37,44] To understand the stronger binding of Cu to the SRE mixture, mixed ligand chelates may form with Cu^{2+}, like an amino-phenolic ligand.[45] Within the mixture, binding between Cu^{2+} and aromatic rings and π-stacking between different components in more complicated geometries may be possible, further contributing to the higher binding affinity.[37,44,46]

Determination of *n*Cu−SRE Thermodynamic Binding Parameters. The nITC thermograms for SRE and four different individual organic acids solution titrated into the *n*Cu suspension are shown in Figure 3. The titration of the other individual SRE components (sugar and amino acids) into the *n*Cu suspension resulted in a low exothermic interaction (Figure S3), similar to the titration of SRE into water, reflecting dilution heat but minimal binding. The interactions between *n*Cu and SRE or these four organic acids are exothermic. Notably, in each thermogram, the first several peaks have a much larger peak area than the rest, indicating a very large heat exchange. Furthermore, it took a longer time for the heat flow signal of the first injection to return to the baseline, featuring a long tail associated with the peak. This indicates there was a strong interaction process at the beginning, followed by many binding interactions induced by the pulse of titrates. The continuous heat exchange reflects the release of Cu^{2+} from the surface of *n*Cu particles via dissolution, which is also an exothermic process and strongly depends on the concentration of H^+ in the environment.[24,47] Thus, when SRE or organic acids are added into the cell, they can bind to the *n*Cu particles or dissolved Cu^{2+} via complexation, and the excess H^+ promotes further dissolution of *n*Cu. There is an important difference in the thermogram of SRE titrating into *n*Cu compared to the titration of the organic acids: for SRE titration the broad peaks were only observed in the first six peaks, which were then followed by sharp peaks. However, for the titration of the individual organic acids, more broad peaks and less sharp peaks were observed. This indicates that SRE can dissolve *n*Cu faster and further than the individual organic acids due to higher $[H^+]$.

The energy exchange as a function of the molar ratio of SRE or organic acids to *n*Cu particles is presented in Figure 4. The corresponding fitted thermodynamic parameters are listed in Table 2. The interactions between *n*Cu and SRE at 298 K are energetically favored spontaneous processes with ΔG ranging from −21.41 to −29.72 kJ/mol, and the interactions are enthalpically driven with negative ΔH values. Negative changes in entropy ($\Delta S < 0$) suggest there could be strong bonds between Cu^{2+} or *n*Cu with hydration water (metal−oxygen bonds), as the entropies of hydration are negative.[48,49] Notably, the stoichiometric values are much smaller than unity (Table 2). Malic acid has the lowest value (n = 0.098), and SRE the highest value (n = 0.336). It is possible that SRE or its components can form bridges or cross-link the *n*Cu particles.[26,27] The bridges or cross-linked structure may restrict further access to the surface of the *n*Cu particles due to conformational hindrance; thus, larger molecules (e.g., malic acid and citric acid) have a smaller n, while smaller ones (e.g., oxalic acid) have larger n. For the SRE mixture, the stoichiometry value is significantly higher than for the individual organic acids since within the mixture several SRE components may bind with the *n*Cu particles simultaneously, involving the following interactions: $n\text{Cu} + A^{2-} + L \rightleftharpoons n\text{CuLA}$, $n\text{Cu} + H^{2-} \rightarrow Cu^{2+}$, $Cu^{2+} + A^{2-} \rightleftharpoons \text{CuA}$, $\text{CuA} + L \rightleftharpoons \text{CuLA}$, and $Cu^{2+} + A^{2-} + L \rightleftharpoons \text{CuLA}$. Since several SRE components can be consumed, the stoichiometric value is larger.

DOI: 10.1021/acs.est.7b02523
Environ. Sci. Technol. XXXX, XXX, XXX−XXX

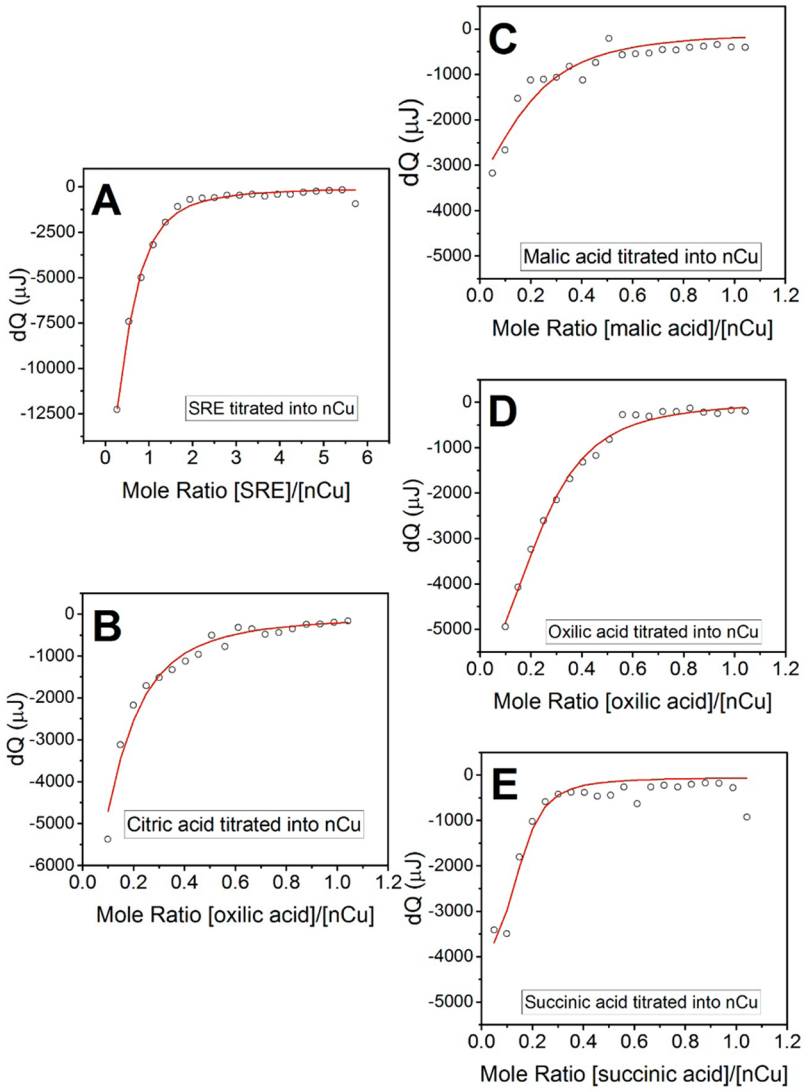

Figure 4. Integrated heat data as a function of molar ratio of (A) SRE, (B) citric acid, (C) malic acid, (D) oxalic acid, and (E) succinic acid to *n*Cu particles, fitted with MNIS model. Symbols represent experimental data, and red lines represent model prediction.

Table 2. MNIS Model Fit of ΔH and n with Confidence Intervals (95% confidence level) from nITC Analysis of the Interaction between SRE or Its Components and *n*Cu and Calculated K_d, ΔG, ΔS, and $-T\Delta S$ from K_a and ΔH Values

Titrate/Ligand	ΔH (kJ/mol)	n	K_d (M^{-1})	ΔG (kJ/mol)	ΔS (J/K mol)	$-T\Delta S$(kJ/mol)
SRE	−77.67 ± 19.57	0.336 ± 0.063	5.645×10^3	−21.41	−188.7	56.26
Oxalic acid	−97.55 ± 13.31	0.220 ± 0.024	1.921×10^4	−24.45	−245.2	73.10
Citric acid	−141.9 ± 47.98	0.122 ± 0.029	1.801×10^4	−24.29	−394.4	117.6
Succinic acid	−56.06 ± 8.290	0.127 ± 0.012	1.607×10^5	−29.72	−88.37	26.35
Malic acid	−83.64 ± 29.37	0.098 ± 0.032	1.299×10^4	−23.48	−201.8	60.16

The affinity to *n*Cu follows the pattern: succinic acid > oxalic acid > citric acid > malic acid > SRE. Succinic acid has the strongest interactions toward *n*Cu particles with a binding constant of 1.61×10^5 M^{-1}, likely from a significant coating of *n*Cu particles since succinic acid is a relatively large molecule. Interestingly, SRE has the weakest binding constant (5.65×10^3 M^{-1}) with *n*Cu particles, while the SRE−Cu^{2+} interaction (Table 1) is the strongest. A likely explanation is that the interaction of SRE with *n*Cu is initially dominated by *n*Cu dissolution (as seen in the first six injections), followed by sorption and chelation in subsequent interactions (after the sixth injection). Thus, a significant fraction of the binding would be between SRE and Cu^{2+}; this is also supported by the fact that the binding constants of SRE−Cu^{2+} (Table 1) and *n*Cu−SRE (Table 2) are similar.

Transformation of *n*Cu in the Presence of SRE. After exposure to SRE, solid *n*Cu particles are present. However, blue fiber-like precipitates were observed after *n*Cu was exposed to citric acid or malic acid and then freeze-dried under vacuum. These fiber-like precipitates are likely to be organic Cu salts. Comparing the XPS survey scans of *n*Cu "as received" to those exposed to SRE or the organic acids (Figure S4), an abundance of C and O atoms was observed in the exposed *n*Cu, which reflect the adsorption of organic acids or SRE components. The

DOI: 10.1021/acs.est.7b02523
Environ. Sci. Technol. XXXX, XXX, XXX−XXX

FTIR spectrum (Figure S6) showed that more functional groups (including C−H, C−O, C═O, and O−H) were detected after *n*Cu was exposed to SRE or organic acids, also suggesting the adsorption or coating of organic acids or SRE onto *n*Cu. High resolution XPS scans of Cu $2p_{3/2}$ peaks of *n*Cu particles or precipitates obtained after 48 h mixing with SRE or individual organic acids are shown in Figure 5 and Figure S5.

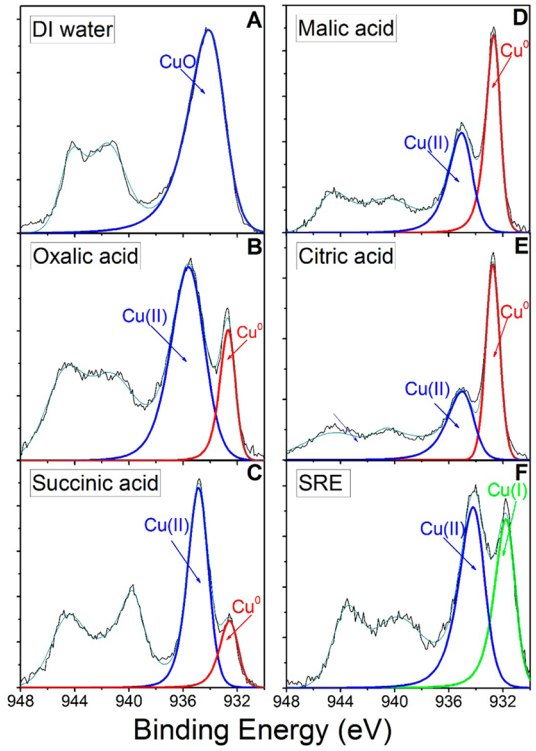

Figure 5. High resolution Cu $2p_{3/2}$ spectra of *n*Cu particles after exposure to (A) DI water, (B) oxalic acid, (C) succinic acid, (D) malic acid, (E) citric acid, and (F) SRE, showing the difference in the abundance of Cu (0), Cu(I), and Cu(II) species.

All of the peaks used to model different Cu species have full width at half-maximum (fwhm) values that are ±0.2 eV. Peaks found at 932.63, 932.18, 933.76, and 934.67 eV are assigned to Cu (0), Cu (I) oxide, Cu (II) oxide, and Cu (II) hydroxide.[50−53]

The fractions of different Cu species in the samples were determined by integrating XPS spectra peak areas (Table S4). Initially, as received (dry) *n*Cu particles contained 11.6% Cu(0), mostly CuO due to atmospheric oxidation (Figure S4). When *n*Cu particles were exposed to DI water, *n*Cu was oxidized further to 100% CuO on the surface (Table S4). XPS can only provide limited information below the surface (~6 nm).[54] In the presence of individual organic acids, there was partial transformation of Cu(II) to Cu(0) on the surface, possibly via dissolution of the protective CuO layer and possibly via reduction. The decreased HDDs and less negative zeta potential values of *n*Cu (Table S6) also indicated the dissolution. Based on solution pH before and after *n*Cu was mixed in, as well as the pK_a of these individual organic acids (Table S5), malic and citric acids release more H^+ than oxalic and succinic acids (also see the less negative ζ values of *n*Cu in Table S6), resulting in greater dissolution extent of *n*Cu (Figure S7). Upon drying, the dissolved Cu ions form the blue fiber-like organic-Cu precipitates.

Notably, Cu(I) was only observed in the sample that interacted with SRE. Cu(I) can be generated from either Cu(0) and Cu(II) via the following reactions:[55]

$$Cu(s) \rightleftharpoons Cu^+ + e^- \ (E^0 = -0.520\,V)$$

$$2Cu(s) + 2OH^- + e^- \rightleftharpoons Cu_2O(s) + H_2O \ (E^0 = +0.360\,V)$$

$$Cu^{2+} + e^- \rightleftharpoons Cu^+ \ (E^0 = +0.159\,V)$$

This suggests that several complex reactions may be involved in the interaction between SRE and *n*Cu.

Bioavailability of Free Cu Ions in Soil Exposed to *n*Cu and SRE. Free Cu^{2+} in soil pore water increased significantly in the presence of *n*Cu and added SRE (Figure 6) or organic acids

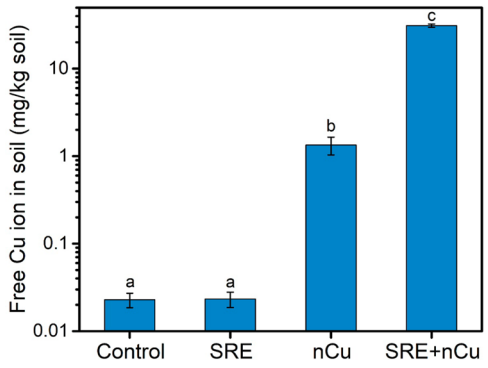

Figure 6. Bioavailability of free Cu ions in the soil in the presence of SRE and *n*Cu. Free Cu ions were determined by the Cu content in the supernatant via ICP-MS. Control is the free Cu in soil water without adding *n*Cu. Data are the mean of four replicates, and error bars represent ± standard error. Different letters stand for statistical differences at $p \leq 0.05$ (Tukey's HSD multiple comparison at $p \leq 0.05$).

(Figure S8). Similar to the study in aqueous suspensions, SRE had a strong dissolution ability resulting in the largest fraction of bioavailable Cu in the soil due to largest pH change in soil pore water before and after mixing SRE with *n*Cu (Table S7). Thus, RE would significantly affect the fate and transport of *n*Cu particles, particularly dissolution and the bioavailability of free Cu ion in the soil systems, which would further result in implications for crop plants.

Cu Bioaccumulation in Cucumber. In previous studies, we demonstrated that copper can be taken up and transported from roots to stems and leaves in cucumber exposed to *n*Cu in the soil.[9−11] In this study, we exposed cucumber plants to soil with *n*Cu and SRE and found that Cu concentrations in cucumber leaves were significantly higher than in the controls with no *n*Cu and no added SRE (Figure 7). However, when the plants were treated with SRE, Cu bioaccumulation in cucumber leaves was hindered, significantly decreasing [Cu]. The carboxyl and amino groups associated with these compounds (Table S1) can act as ligands to chelate Cu.[56] Previous studies have suggested that amino acids in xylem sap can bind Cu efficiently.[57−60] The complexation of Cu by SRE components (amino acids or organic acids) may contribute to limit translocation of Cu to leaves.

DOI: 10.1021/acs.est.7b02523
Environ. Sci. Technol. XXXX, XXX, XXX−XXX

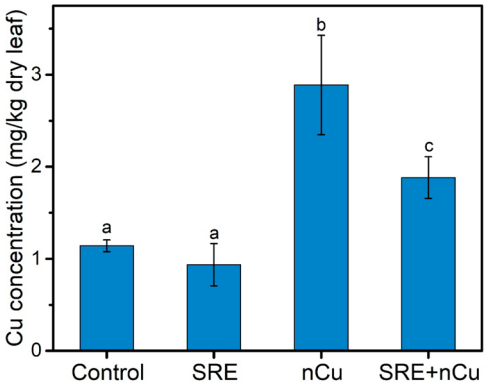

Figure 7. Cu concentration in cucumber leaves at harvest for plants grown in soil spiked with different combinations of *n*Cu and SRE. Data are the mean of four replicates, and error bars represent ± standard error. Different letters stand for statistical differences at $p \leq 0.05$ (Tukey's HSD multiple comparison at $p \leq 0.05$).

ENVIRONMENTAL SIGNIFICANCE

nITC was applied to measure the fundamental thermodynamics of the interactions between *n*Cu or the Cu ion and SRE and its major components. While Cu^{2+} interacts most strongly with three amino acids (leucine, proline, and serine) and oxalic acid, *n*Cu interacted mostly with small organic acids. Stronger interactions between the SRE mixture and Cu^{2+} indicated a mixed ligand chelation. The interaction with the organic acids led to dissolution of the *n*Cu surface, removing CuO that had formed on the original *n*Cu particles. It is also possible that some reduction occurred at the *n*Cu surface. Although *n*Cu dissolution was determined to be a predominant interaction in soil, individual SRE compounds (e.g., succinic acid) can also affect the state of *n*Cu via coating or bridging. The interactions presented in this study serve to better understand the initial transformation of *n*Cu and the interactions between *n*Cu or Cu^{2+} and the various SRE components. However, we did not study the role of the microbiome in the rhizosphere, which may alter the levels of SRE components and lead to different or additional interactions.

The bioavailability of free Cu in soils exposed to *n*Cu and SRE increased significantly, which has implications for soil organisms (e.g., microbes, worms, other invertebrates). On the other hand, plants exposed to soil with *n*Cu and added SRE had significantly less translocation of Cu to the leaves and upper plant tissues.

ASSOCIATED CONTENT

Supporting Information

The Supporting Information is available free of charge on the ACS Publications website at DOI: 10.1021/acs.est.7b02523.

Figure S1: SEM and TEM image of *n*Cu. Section S2: SRE components and concentrations. Section S3: nITC analysis model and method. Figures S2 and S3: Real-time thermogram for Cu^{2+}/*n*Cu and individual SRE compounds. Figures S4 and S5: XPS scan of *n*Cu. Figure S6: FTIR spectrum of *n*Cu. Figures S7 and S8: Dissolution extent of *n*Cu. Table S4: Fraction of different states of Cu. Table S6: HDD and zeta potential of *n*Cu. Tables S5 and S7: Solution pH change. (PDF)

AUTHOR INFORMATION

Corresponding Author

*Tel: +1 805 893 7548. Fax: +1 805 893 7612. E-mail: keller@bren.ucsb.edu.

ORCID

Yuxiong Huang: 0000-0001-8124-643X
Lijuan Zhao: 0000-0002-5869-8769
Arturo A. Keller: 0000-0002-7638-662X

Notes

The authors declare no competing financial interest.

ACKNOWLEDGMENTS

This work was supported by the National Science Foundation (NSF) and the U.S. Environmental Protection Agency (EPA) under NSF-EF0830117. Any opinions, findings, conclusions, or recommendations expressed in this material are those of the authors and do not necessarily reflect the views of the funding agencies. The MRL Central Facilities are supported by the MRSEC Program of the National Science Foundation under awards No. DMR 1121053; a member of the NSF-funded Materials Research Facilities Network (www.mrfn.org). We thank the MRL Central Facilities for the use of their nITC, FTIR, and XPS instruments as well as Dr. Tom Mates at the UCSB MRL for his help with XPS measurements. A.A.K. also appreciates Agilent Technologies for their Agilent Thought Leader Award.

REFERENCES

(1) Lee, Y.; Choi, J.-r.; Lee, K. J.; Stott, N. E.; Kim, D. Large-scale synthesis of copper nanoparticles by chemically controlled reduction for applications of inkjet-printed electronics. *Nanotechnology* **2008**, *19* (41), 415604.

(2) Adeleye, A. S.; Oranu, E. A.; Tao, M.; Keller, A. A. Release and detection of nanosized copper from a commercial antifouling paint. *Water Res.* **2016**, *102*, 374−82.

(3) Adeleye, A. S.; Conway, J. R.; Garner, K.; Huang, Y. X.; Su, Y. M.; Keller, A. A. Engineered nanomaterials for water treatment and remediation: Costs, benefits, and applicability. *Chem. Eng. J.* **2016**, *286*, 640−662.

(4) Khot, L. R.; Sankaran, S.; Maja, J. M.; Ehsani, R.; Schuster, E. W. Applications of nanomaterials in agricultural production and crop protection: A review. *Crop Prot.* **2012**, *35*, 64−70.

(5) Keller, A. A.; McFerran, S.; Lazareva, A.; Suh, S. Global life cycle releases of engineered nanomaterials. *J. Nanopart. Res.* **2013**, *15* (6), 1692.

(6) Conway, J. R.; Adeleye, A. S.; Gardea-Torresdey, J.; Keller, A. A. Aggregation, Dissolution, and Transformation of Copper Nanoparticles in Natural Waters. *Environ. Sci. Technol.* **2015**, *49* (5), 2749−2756.

(7) Adeleye, A. S.; Conway, J. R.; Perez, T.; Rutten, P.; Keller, A. A. Influence of Extracellular Polymeric Substances on the Long-Term Fate, Dissolution, and Speciation of Copper-Based Nanoparticles. *Environ. Sci. Technol.* **2014**, *48* (21), 12561−12568.

(8) Zhao, L.; Ortiz, C.; Adeleye, A. S.; Hu, Q.; Zhou, H.; Huang, Y.; Keller, A. A. Metabolomics to Detect Response of Lettuce (Lactuca sativa) to Cu(OH)2 Nano-pesticides: Oxidative Stress Response and Detoxification Mechanisms. *Environ. Sci. Technol.* **2016**, *50* (17), 9697−707.

(9) Zhao, L.; Huang, Y.; Zhou, H.; Adeleye, A. S.; Wang, H.; Ortiz, C.; Mazer, S.; Keller, A. A. GC-TOF-MS based metabolomics and ICP-MS based metallomics of cucumber (Cucumis sativus) fruits reveal alteration of metabolites profile and biological pathway disruption induced by nano copper. *Environ. Sci.: Nano* **2016**, *3* (5), 1114−1123.

DOI: 10.1021/acs.est.7b02523
Environ. Sci. Technol. XXXX, XXX, XXX−XXX

(10) Zhao, L.; Huang, Y.; Hu, J.; Zhou, H.; Adeleye, A. S.; Keller, A. A. 1H NMR and GC-MS Based Metabolomics Reveal Defense and Detoxification Mechanism of Cucumber Plant under Nano-Cu Stress. *Environ. Sci. Technol.* **2016**, *50* (4), 2000−2010.
(11) Zhao, L.; Hu, J.; Huang, Y.; Wang, H.; Adeleye, A.; Ortiz, C.; Keller, A. A. 1H NMR and GC-MS based metabolomics reveal nano-Cu altered cucumber (Cucumis sativus) fruit nutritional supply. *Plant Physiol. Biochem.* **2017**, *110*, 138−146.
(12) Keller, A. A.; Adeleye, A. S.; Conway, J. R.; Garner, K. L.; Zhao, L.; Cherr, G. N.; Hong, J.; Gardea-Torresdey, J. L.; Godwin, H. A.; Hanna, S.; Ji, Z.; Kaweeteerawat, C.; Lin, S.; Lenihan, H. S.; Miller, R. J.; Nel, A. E.; Peralta-Videa, J. R.; Walker, S. L.; Taylor, A. A.; Torres-Duarte, C.; Zink, J. I.; Zuverza-Mena, N. Comparative environmental fate and toxicity of copper nanomaterials. *NanoImpact* **2017**, *7*, 28−40.
(13) Zhao, L.; Hu, Q.; Huang, Y.; Fulton, A.; Hannah-Bick, C.; Adeleye, A.; Keller, A. A. Activation of Antioxidant and Detoxification Gene Expression in Cucumber Plants Exposed to a $Cu(OH)_2$ Nanopesticide. *Environ. Sci.: Nano* **2017**, *4*, 1750−1760.
(14) Zhao, L.; Huang, Y.; Hannah-Bick, C.; Fulton, A. N.; Keller, A. A. Application of metabolomics to assess the impact of Cu(OH)2 nanopesticide on the nutritional value of lettuce (Lactuca sativa): Enhanced Cu intake and reduced antioxidants. *NanoImpact* **2016**, *3*−*4*, 58−66.
(15) Zhao, L.; Huang, Y.; Adeleye, A. S.; Keller, A. A. Metabolomics Reveals Cu(OH)2 Nanopesticide Activated Antioxidative Pathways and Decreased Beneficial Antioxidants in Spinach Leaves. *Environ. Sci. Technol.* **2017**, na.
(16) Hogberg, P.; Nordgren, A.; Buchmann, N.; Taylor, A. F. S.; Ekblad, A.; Hogberg, M. N.; Nyberg, G.; Ottosson-Lofvenius, M.; Read, D. J. Large-scale forest girdling shows that current photosynthesis drives soil respiration. *Nature* **2001**, *411* (6839), 789−792.
(17) Clemmensen, K. E.; Bahr, A.; Ovaskainen, O.; Dahlberg, A.; Ekblad, A.; Wallander, H.; Stenlid, J.; Finlay, R. D.; Wardle, D. A.; Lindahl, B. D. Roots and Associated Fungi Drive Long-Term Carbon Sequestration in Boreal Forest. *Science* **2013**, *339* (6127), 1615−1618.
(18) Badri, D. V.; Vivanco, J. M. Regulation and function of root exudates. *Plant, Cell Environ.* **2009**, *32* (6), 666−681.
(19) Walker, T. S.; Bais, H. P.; Grotewold, E.; Vivanco, J. M. Root exudation and rhizosphere biology. *Plant Physiol.* **2003**, *132* (1), 44−51.
(20) LeFevre, G. H.; Hozalski, R. M.; Novak, P. J. Root exudate enhanced contaminant desorption: an abiotic contribution to the rhizosphere effect. *Environ. Sci. Technol.* **2013**, *47* (20), 11545−53.
(21) Servin, A. D.; White, J. C. Nanotechnology in agriculture: Next steps for understanding engineered nanoparticle exposure and risk. *NanoImpact* **2016**, *1*, 9−12.
(22) Keller, A. A.; Wang, H. T.; Zhou, D. X.; Lenihan, H. S.; Cherr, G.; Cardinale, B. J.; Miller, R.; Ji, Z. X. Stability and Aggregation of Metal Oxide Nanoparticles in Natural Aqueous Matrices. *Environ. Sci. Technol.* **2010**, *44* (6), 1962−1967.
(23) Bennett, S. W.; Adeleye, A.; Ji, Z. X.; Keller, A. A. Stability, metal leaching, photoactivity and toxicity in freshwater systems of commercial single wall carbon nanotubes. *Water Res.* **2013**, *47* (12), 4074−4085.
(24) Miao, A. J.; Zhang, X. Y.; Luo, Z. P.; Chen, C. S.; Chin, W. C.; Santschi, P. H.; Quigg, A. Zinc Oxide Engineered Nanoparticles Dissolution and Toxicity to Marine Phytoplankton. *Environ. Toxicol. Chem.* **2010**, *29* (12), 2814−2822.
(25) Peralta-Videa, J. R.; Huang, Y.; Parsons, J. G.; Zhao, L.; Lopez-Moreno, L.; Hernandez-Viezcas, J. A.; Gardea-Torresdey, J. L. Plant-based green synthesis of metallic nanoparticles: scientific curiosity or a realistic alternative to chemical synthesis? *Nanotechnol. Environ. Eng.* **2016**, *1* (1), 1−29.
(26) Loosli, F.; Vitorazi, L.; Berret, J.-F.; Stoll, S. Isothermal titration calorimetry as a powerful tool to quantify and better understand agglomeration mechanisms during interaction processes between TiO2 nanoparticles and humic acids. *Environ. Sci.: Nano* **2015**, *2* (5), 541−550.
(27) Loosli, F.; Vitorazi, L.; Berret, J.-F.; Stoll, S. Towards a better understanding on agglomeration mechanisms and thermodynamic properties of TiO2 nanoparticles interacting with natural organic matter. *Water Res.* **2015**, *80*, 139−148.
(28) Huang, Y.; Keller, A. A. Isothermal titration microcalorimetry to determine the thermodynamics of metal ion removal by magnetic nanoparticle sorbents. *Environ. Sci.: Nano* **2016**, *3* (5), 1206−1214.
(29) Ghai, R.; Falconer, R. J.; Collins, B. M. Applications of isothermal titration calorimetry in pure and applied research—survey of the literature from 2010. *J. Mol. Recognit.* **2012**, *25* (1), 32−52.
(30) Grayston, S. J.; Vaughan, D.; Jones, D. Rhizosphere carbon flow in trees, in comparison with annual plants: The importance of root exudation and its impact on microbial activity and nutrient availability. *Appl. Soil Ecol.* **1997**, *5* (1), 29−56.
(31) Turnbull, W. B.; Daranas, A. H. On the value of c: can low affinity systems be studied by isothermal titration calorimetry? *J. Am. Chem. Soc.* **2003**, *125* (48), 14859−14866.
(32) Lazareva, A.; Keller, A. A. Estimating potential life cycle releases of engineered nanomaterials from wastewater treatment plants. *ACS Sustainable Chem. Eng.* **2014**, *2* (7), 1656−1665.
(33) Conway, J. R.; Beaulieu, A. L.; Beaulieu, N. L.; Mazer, S. J.; Keller, A. A. Environmental Stresses Increase Photosynthetic Disruption by Metal Oxide Nanomaterials in a Soil-Grown Plant. *ACS Nano* **2015**, *9* (12), 11737−49.
(34) *Method 3051A: Microwave Assisted Acid Digestion of Sediments, Sludges, Soils, and Oils*; U.S. Environmental Protection Agency, 2007.
(35) Zhao, L. J.; Sun, Y. P.; Hernandez-Viezcas, J. A.; Servin, A. D.; Hong, J.; Niu, G. H.; Peralta-Videa, J. R.; Duarte-Gardea, M.; Gardea-Torresdey, J. L. Influence of CeO2 and ZnO Nanoparticles on Cucumber Physiological Markers and Bioaccumulation of Ce and Zn: A Life Cycle Study. *J. Agric. Food Chem.* **2013**, *61* (49), 11945−11951.
(36) Freire, E.; Mayorga, O. L.; Straume, M. Isothermal titration calorimetry. *Anal. Chem.* **1990**, *62* (18), 950A−959A.
(37) de Bruin, T. J. M.; Marcelis, A. T. M.; Zuilhof, H.; Sudholter, E. J. R. Enantioselectivity measurements of copper(II) amino acid complexes using isothermal titration calorimetry. *Langmuir* **2000**, *16* (22), 8270−8275.
(38) De Bruin, T. J.; Marcelis, A.; Zuilhof, H.; Rodenburg, L. M.; Niederländer, H. A.; Koudijs, A.; Overdevest, P. E.; Padt, A. V. D.; Sudhölter, E. J. Separation of amino acid enantiomers by micelle-enhanced ultrafiltration. *Chirality* **2000**, *12* (8), 627−636.
(39) Pliska, V.; Schmidt, M.; Fauchere, J. L. Partition-Coefficients of Amino-Acids and Hydrophobic Parameters-Pi of Their Side-Chains as Measured by Thin-Layer Chromatography. *J. Chromatogr.* **1981**, *216* (Oct), 79−92.
(40) McAuley, A.; Nancollas, G. Complex formation in solutions of copper oxalate. *Trans. Faraday Soc.* **1960**, *56*, 1165−1171.
(41) L'Heureux, G. A.; Martell, A. E. Mixed ligand chelates of copper(II). *J. Inorg. Nucl. Chem.* **1966**, *28* (2), 481−491.
(42) Hallman, P.; Perrin, D.; Watt, A. E. The computed distribution of copper (II) and zinc (II) ions among seventeen amino acids present in human blood plasma. *Biochem. J.* **1971**, *121* (3), 549−555.
(43) Chidambaram, M. V.; Bhattacharya, P. K. Studies in amine-amino acid mixed ligand chelates—I. *J. Inorg. Nucl. Chem.* **1970**, *32* (10), 3271−3275.
(44) de Bruin, T. J. M.; Marcelis, A. T. M.; Zuilhof, H.; Sudholter, E. J. R. Geometry and electronic structure of bis-(glycinato)-CuII[middle dot]2H2O complexes as studied by density functional B3LYP computations. *Phys. Chem. Chem. Phys.* **1999**, *1* (18), 4157−4163.
(45) Dapporto, P.; Formica, M.; Fusi, V.; Giorgi, L.; Micheloni, M.; Paoli, P.; Pontellini, R.; Rossi, P. Addition of small molecules by Zn(II) and Cu(II) dinuclear complexes obtained by an amino-phenolic ligand. Crystal structures of the dinuclear zinc complex assembling butanolate and azide anions. *Inorg. Chem.* **2001**, *40* (24), 6186−6192.
(46) Yamauchi, O.; Odani, A. Structure-Stability Relationship in Ternary Copper(Ii) Complexes Involving Aromatic-Amines and Tyrosine or Related Amino-Acids - Intramolecular Aromatic Ring

DOI: 10.1021/acs.est.7b02523
Environ. Sci. Technol. XXXX, XXX, XXX−XXX

Stacking and Its Regulation through Tyrosine Phosphorylation. *J. Am. Chem. Soc.* **1985**, *107* (21), 5938−5945.
(47) Rimer, J. D.; Trofymluk, O.; Navrotsky, A.; Lobo, R. F.; Vlachos, D. G. Kinetic and thermodynamic studies of silica nanoparticle dissolution. *Chem. Mater.* **2007**, *19* (17), 4189−4197.
(48) de Namor, A. F. D.; Tanaka, D. A. P. Thermodynamics of protonation and complexation of EDTA derivatives and metal cations in water. *J. Chem. Soc., Faraday Trans.* **1998**, *94* (20), 3105−3110.
(49) Wright, D. L.; Holloway, J. H.; Reilley, C. N. Heats and Entropies of Formation of Metal Chelates of Polyamine and Polyaminocarboxylate Ligands. *Anal. Chem.* **1965**, *37* (7), 884−892.
(50) Biesinger, M. C.; Lau, L. W.; Gerson, A. R.; Smart, R. S. C. Resolving surface chemical states in XPS analysis of first row transition metals, oxides and hydroxides: Sc, Ti, V, Cu and Zn. *Appl. Surf. Sci.* **2010**, *257* (3), 887−898.
(51) Goh, S. W.; Buckley, A. N.; Lamb, R. N.; Rosenberg, R. A.; Moran, D. The oxidation states of copper and iron in mineral sulfides, and the oxides formed on initial exposure of chalcopyrite and bornite to air. *Geochim. Cosmochim. Acta* **2006**, *70* (9), 2210−2228.
(52) Poulston, S.; Parlett, P.; Stone, P.; Bowker, M. Surface oxidation and reduction of CuO and Cu2O studied using XPS and XAES. *Surf. Interface Anal.* **1996**, *24* (12), 811−820.
(53) Wagner, C. D.; Naumkin, A. V.; Kraut-Vass, A.; Allison, J. W.; Powell, C. J.; Rumble, J. R., Jr. *NIST Standard Reference Database 20*; NIST XPS Database Version 3, 2003; pp 251−252.
(54) Yan, W.; Ramos, M. A.; Koel, B. E.; Zhang, W.-x. As (III) sequestration by iron nanoparticles: study of solid-phase redox transformations with X-ray photoelectron spectroscopy. *J. Phys. Chem. C* **2012**, *116* (9), 5303−5311.
(55) Bard, A. J.; Parsons, R.; Jordan, J. *Standard Potentials in Aqueous Solution*; CRC Press, 1985; Vol. *6*.
(56) Hossain, M. A.; Piyatida, P.; da Silva, J. A. T.; Fujita, M. Molecular mechanism of heavy metal toxicity and tolerance in plants: central role of glutathione in detoxification of reactive oxygen species and methylglyoxal and in heavy metal chelation. *J. Bot.* **2012**, *2012*, 1−37.
(57) GRAHAM, R. D. Transport of copper and manganese to the xylem exudate of sunflower. *Plant, Cell Environ.* **1979**, *2* (2), 139−143.
(58) White, M. C.; Chaney, R. L.; Decker, A. M. Metal complexation in xylem fluid III. Electrophoretic evidence. *Plant Physiol.* **1981**, *67* (2), 311−315.
(59) Pich, A.; Scholz, G. Translocation of copper and other micronutrients in tomato plants (Lycopersicon esculentum Mill.): nicotianamine-stimulated copper transport in the xylem. *J. Exp. Bot.* **1996**, *47* (1), 41−47.
(60) Liao, M.; Hedley, M.; Woolley, D.; Brooks, R.; Nichols, M. Copper uptake and translocation in chicory (Cichorium intybus L. cv Grasslands Puna) and tomato (Lycopersicon esculentum Mill. cv Rondy) plants grown in NFT system. II. The role of nicotianamine and histidine in xylem sap copper transport. *Plant Soil* **2000**, *223* (1−2), 245−254.

DOI: 10.1021/acs.est.7b02523
Environ. Sci. Technol. XXXX, XXX, XXX−XXX